

High-Speed Algorithm for Shielding Current Analysis in HTS Film with Cracks^{*)}

Atsushi KAMITANI, Teruou TAKAYAMA, Ayumu SAITOH¹⁾ and Hiroaki NAKAMURA²⁾

Yamagata University, 4-3-16 Johnan, Yonezawa, Yamagata 992-8510, Japan

¹⁾*University of Hyogo, 2167 Shosha, Himeji, Hyogo 671-2280, Japan*

²⁾*National Institute of Fusion Science, 322-6 Oroshi, Toki, Gifu 509-5292, Japan*

(Received 23 November 2014 / Accepted 17 February 2015)

A fast and stable method is proposed for calculating the time-varying shielding current density in a high-temperature superconducting (HTS) film containing cracks. If an initial-boundary-value problem of the shielding current density is formulated by the T -method, integral forms of Faraday's law on crack surfaces are also imposed as boundary conditions. As a result of the spatial discretization of the initial-boundary-value problem, semi-explicit differential algebraic equations (DAEs) are obtained. Although the DAEs can be solved with standard ordinary-differential-equation (ODE) solvers, much CPU time is required for their numerical solution. In order to shorten the CPU time, the following high-speed algorithm is proposed: the block LU decomposition is incorporated into function evaluations in ODE solvers. A numerical code is developed on the basis of the proposed algorithm and detectability of cracks by the scanning permanent-magnet method is numerically investigated. The results of computations show that, when multiple cracks is contained in an HTS film, resolution of the scanning permanent-magnet method will be degraded remarkably.

© 2015 The Japan Society of Plasma Science and Nuclear Fusion Research

Keywords: block LU decomposition, critical current density, high-temperature superconductor, integrodifferential equation, surface crack

DOI: 10.1585/pfr.10.3405023

1. Introduction

Recently, a high-temperature superconductor (HTS) has been used for numerous engineering applications: magnet, energy storage system, power cable and magnetic shielding apparatus. Since the evaluation of the shielding current density is indispensable for the design of engineering applications, several numerical methods [1–3] have been so far proposed to calculate the shielding current density.

After discretized with the implicit scheme and the finite element method (FEM), an initial-boundary-value problem of the shielding current density is transformed to a problem in which nonlinear algebraic equations have to be solved at each time step. Although this method can be also applied to the shielding current analysis in an HTS film containing cracks [3, 4], it is extremely time-consuming. Such time consumption is caused by a linear term with a dense matrix in the nonlinear equations. This method is called a conventional method, hereafter.

The authors proposed a high-speed method [2] for calculating the shielding current density in an HTS film. After discretized with the FEM, the initial-boundary-value problem reduces to a system of first-order ordinary differential equations (ODEs) that has a strong nonlinearity. How-

ever, the system cannot be always solved by means of an ODE solver even when an adaptive step-size control algorithm [5] is incorporated to the solver. In order to suppress an overflow in the algorithm, the J - E constitutive relation is slightly modified so that its solution may satisfy the original constitutive relation. As a result, the proposed method has a much higher speed than the conventional one. However, the method is not applicable to the case where cracks are contained in an HTS film. This is mainly because the spatial discretization of the initial-boundary-value problem yields differential algebraic equations (DAEs) for this case.

The purpose of the present study is to develop a fast and stable method for analyzing the shielding current density in an HTS film containing cracks and to numerically investigate the scanning permanent-magnet method (SPM) [6] by means of the method.

2. Governing Equations

We first assume that an HTS film has the same cross section Ω over the thickness and that it is exposed to the time-varying magnetic field \mathbf{B}/μ_0 . By taking its thickness direction as z -axis and choosing its centroid as the origin, we use the Cartesian coordinate system $\langle O : \mathbf{e}_x, \mathbf{e}_y, \mathbf{e}_z \rangle$. Furthermore, the HTS film is assumed to contain cracks whose cross sections are curved segments in the xy plane. Note that the boundary $\partial\Omega$ of Ω is composed of not only the outer boundary C_0 but also the inner boundaries

author's e-mail: kamitani@yz.yamagata-u.ac.jp

^{*)} This article is based on the presentation at the 24th International Toki Conference (ITC24).

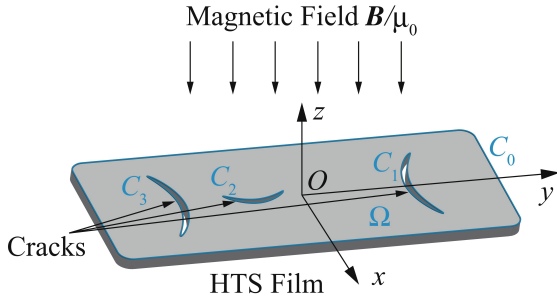


Fig. 1 An HTS film containing cracks.

C_1, C_2, \dots, C_m . Apparently, C_1, C_2, \dots, C_m denote crack surfaces (see Fig. 1). In the following, \mathbf{x} and \mathbf{x}' denote position vectors of two points in the xy plane, whereas \mathbf{t} and \mathbf{n} are a unit tangent vector and a unit normal vector on $\partial\Omega$, respectively. In addition, b denotes a thickness of the HTS film.

In HTS films, the electric field \mathbf{E} and the shielding current density \mathbf{j} are closely related to each other through the J - E constitutive relation. As the relation, we assume the following power law [2–4, 7, 8]:

$$\mathbf{E} = E(|\mathbf{j}|) \frac{\mathbf{j}}{|\mathbf{j}|}, \quad E(j) = E_C \left(\frac{j}{j_C} \right)^N,$$

where j_C and E_C denote the critical current density and the critical electric field, respectively, and N is a positive constant.

Under the thin-plate approximation, there exists a scalar function $T(\mathbf{x}, t)$ such that $\mathbf{j} = (2/b)\nabla \times (T\mathbf{e}_z)$ and its time evolution is governed by the following integrodifferential equation [1–4]:

$$\mu_0 \partial_t \langle \hat{W}T \rangle = -\mathbf{e}_z \cdot (\nabla \times \mathbf{E}) - \partial_t \langle \mathbf{B} \cdot \mathbf{e}_z \rangle. \quad (1)$$

Here, $\langle \cdot \rangle$ denotes an average operator over the thickness and \hat{W} is the operator defined by

$$\hat{W}T \equiv \frac{2T(\mathbf{x}, t)}{b} + \iint_{\Omega} Q(|\mathbf{x} - \mathbf{x}'|) T(\mathbf{x}', t) d^2\mathbf{x}',$$

where $Q(r) = -(\pi b^2)^{-1} [r^{-1} - (r^2 + b^2)^{-1/2}]$. Incidentally, (1) is derived from Faraday's law. In other words, (1) is equivalent to Faraday's law under the thin-plate approximation.

The initial and boundary conditions to (1) are assumed as follows:

$$T = 0 \text{ at } t = 0, \quad (2)$$

$$T \in H(\bar{\Omega}), \quad (3)$$

$$h_i(\mathbf{E}) \equiv \oint_{C_i} \mathbf{E} \cdot \mathbf{t} ds = 0 \quad (i = 1, 2, \dots, m). \quad (4)$$

Here, $H(\bar{\Omega})$ is a function space defined by $H(\bar{\Omega}) \equiv \{w(\mathbf{x}) : w = 0 \text{ on } C_0, \partial w / \partial s = 0 \text{ on } C_1, C_2, \dots, C_m\}$, and s is an arclength along crack surfaces C_1, C_2, \dots, C_m . Equation (3) is based on $\mathbf{j} \cdot \mathbf{n} = 0$ on C_0, C_1, \dots, C_m . In contrast, (4)

is integral forms of Faraday's law on crack surfaces and it assures uniqueness of the initial-boundary-value problem of (1).

By solving (1) together with the initial and boundary conditions, we can investigate the time evolution of $T(\mathbf{x}, t)$. Once $T(\mathbf{x}, t)$ is determined at a certain time, the shielding current density at the same time can be easily evaluated by using $\mathbf{j} = (2/b)\nabla \times (T\mathbf{e}_z)$.

3. Numerical Methods

For the purpose of solving the initial-boundary-value problem of (1), the authors developed the virtual voltage method [3]. However, it costs much CPU time. In order to resolve this difficulty, a new method is proposed. In this section, the proposed method is explained in detail and its speed is compared with that of the virtual voltage method.

After spatially discretized with the FEM, the initial-boundary-value problem of (1) is transformed to the following semi-explicit DAEs:

$$\begin{bmatrix} W_{11} & W_{12} \end{bmatrix} \frac{d\mathbf{T}}{dt} = \mathbf{f}_1(t, \mathbf{T}), \quad (5)$$

$$\mathbf{g}(\mathbf{T}) = \mathbf{0}, \quad (6)$$

where $\mathbf{T} \in \mathbb{R}^n$ is a nodal vector originating from $T(\mathbf{x}, t)$ and $\mathbf{f}_1(t, \mathbf{T}) \in \mathbb{R}^{n-m}$ is a vector calculated from the right-hand side of (1). Here, n denotes a total number of nodes and it is assumed to satisfy $n \gg m$. In addition, W_{11} and W_{12} are an $(n-m) \times (n-m)$ matrix and an $(n-m) \times m$ matrix, respectively, and they correspond to the operator \hat{W} . Furthermore, (6) is a discretized form of (4) and, hence, $\mathbf{g}(\mathbf{T})$ is an m -dimensional vector. Note that (5) is derived from (1) and (3). Thus, (5) also contains the boundary condition (3).

Since (5) and (6) show the index-1 property, they can be rewritten as the following ODEs:

$$\frac{d\mathbf{T}}{dt} = \mathbf{f}(t, \mathbf{T}), \quad (7)$$

where $\mathbf{f}(t, \mathbf{T}) \in \mathbb{R}^n$ is defined by

$$W(\mathbf{T})\mathbf{f}(t, \mathbf{T}) = \mathbf{f}^*(t, \mathbf{T}). \quad (8)$$

Here, $W(\mathbf{T})$ and $\mathbf{f}^*(t, \mathbf{T})$ are given by

$$W(\mathbf{T}) = \begin{bmatrix} W_{11} & W_{12} \\ W_{21}(\mathbf{T}) & W_{22}(\mathbf{T}) \end{bmatrix}, \quad (9)$$

$$\mathbf{f}^*(t, \mathbf{T}) = \begin{bmatrix} \mathbf{f}_1(t, \mathbf{T}) \\ \mathbf{0} \end{bmatrix}. \quad (10)$$

In addition, $W_{21}(\mathbf{T})$ and $W_{22}(\mathbf{T})$ are an $m \times (n-m)$ matrix and an $m \times m$ matrix, respectively, and they are given by $[W_{12}(\mathbf{T}) \quad W_{22}(\mathbf{T})] = \partial \mathbf{g} / \partial \mathbf{T}$, where $\partial \mathbf{g} / \partial \mathbf{T}$ is a Jacobian matrix. In the present study, the initial-value problem of (7) is numerically solved by means of the 5th-order Runge-Kutta method with Fehlberg's adaptive step-size control algorithm [5].

In the 5th-order Runge-Kutta method, 6 evaluations of $f(t, \mathbf{T})$ are needed at each time step. In other words, 6 linear systems such as (8) have to be solved for $f(t, \mathbf{T})$ at each time step. As is apparent from the definition of $W(\mathbf{T})$, the submatrices, W_{11} and W_{12} , of $W(\mathbf{T})$ do not depend on \mathbf{T} . Hence, high-speed solution of the linear system (8) can be realized by using the block LU decomposition of $W(\mathbf{T})$.

Suppose $W(\mathbf{T})$ can be written as a product of two matrices,

$$\begin{aligned} W(\mathbf{T}) &= \begin{bmatrix} L_{11} & O \\ L_{21}(\mathbf{T}) & L_{22}(\mathbf{T}) \end{bmatrix} \begin{bmatrix} U_{11} & U_{12} \\ O & U_{22}(\mathbf{T}) \end{bmatrix} \\ &\equiv L(\mathbf{T})U(\mathbf{T}). \end{aligned} \quad (11)$$

Here, L_{11} , $L_{22}(\mathbf{T})$ and $L(\mathbf{T})$ are lower triangular matrices whereas U_{11} , $U_{22}(\mathbf{T})$ and $U(\mathbf{T})$ are upper triangular matrices. In addition, $L_{21}(\mathbf{T})$ and U_{12} are an $m \times (n - m)$ matrix and an $(n - m) \times m$ matrix, respectively. By substituting (9) into (11), we get

$$W_{11} = L_{11}U_{11}, \quad (12)$$

$$W_{12} = L_{11}U_{12}, \quad (13)$$

$$W_{21}(\mathbf{T}) = L_{21}(\mathbf{T})U_{11}, \quad (14)$$

$$W_{22}(\mathbf{T}) - L_{21}(\mathbf{T})U_{12} = L_{22}(\mathbf{T})U_{22}(\mathbf{T}). \quad (15)$$

Thus, the block LU decomposition of $W(\mathbf{T})$ can be achieved by using the following four steps:

1. A submatrix W_{11} is LU decomposed to get L_{11} and U_{11} .
2. Equation (13) is solved for U_{12} .
3. Equation (14) is solved for $L_{21}(\mathbf{T})$.
4. An $m \times m$ matrix $W_{22}(\mathbf{T}) - L_{21}(\mathbf{T})U_{12}$ is LU decomposed to get $L_{22}(\mathbf{T})$ and $U_{22}(\mathbf{T})$.

Note that, even if the nodal vector \mathbf{T} is unknown, both step 1 and step 2 are executable. In contrast, it is not until \mathbf{T} is evaluated that both step 3 and step 4 can be carried out. In other words, step 1 and step 2 have to be only once executed before the numerical solution of (7) is started. On the other hand, the remaining two steps must be performed at every evaluation of $f(t, \mathbf{T})$.

Once the LU decomposition (11) of $W(\mathbf{T})$ is obtained, we can easily solve the linear system (8). Specifically, $L(\mathbf{T})f^\dagger(t, \mathbf{T}) = f^*(t, \mathbf{T})$ is first solved for $f^\dagger(t, \mathbf{T})$ and $U(\mathbf{T})f(t, \mathbf{T}) = f^\dagger(t, \mathbf{T})$ is subsequently solved for $f(t, \mathbf{T})$. Thus, not only step 3 and step 4 but also the numerical solutions of two linear systems are needed for each evaluation of $f(t, \mathbf{T})$. Therefore, if we have already obtained L_{11} , U_{11} and U_{12} , $O((m + 2)n^2)$ operations are required for calculating $f(t, \mathbf{T})$. This means that only $O((m + 2)n^2)$ operations are needed at each time step of the proposed method. In contrast, $O(n^3)$ operations are necessary at each time step of the virtual voltage method. Therefore, the proposed method is expected to have a much higher speed than the virtual voltage method.

Let us compare the speed of the proposed method with that of the virtual voltage method. To this end, the

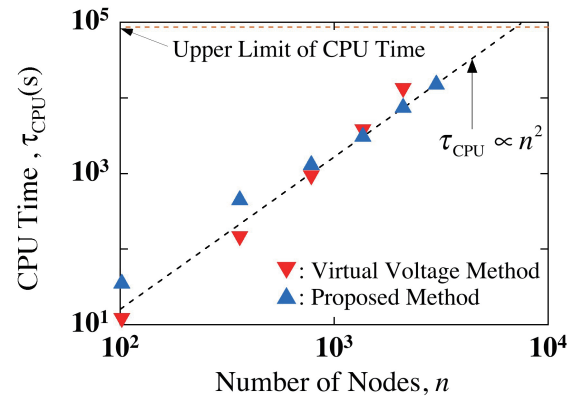


Fig. 2 The CPU time τ_{CPU} as functions of the number n of nodes for the case with $m = 1$. Here, τ_{CPU} is measured for the simulation of the SPM in which values of parameters in Section 4.1 are used.

CPU times τ_{CPU} required for both methods are measured on HITACHI SR16000/XM1 POWER7 of LHD Numerical Analysis Server in National Institute of Fusion Science. The dependence of the CPU time on the number of nodes is depicted in Fig. 2. As expected, the proposed method is faster than the virtual voltage method for the case with $n \gtrsim 10^3$. Especially, for the case with $n = 3007$, the execution of the virtual voltage method was forced to be terminated because the CPU time had exceeded the upper limit, 8.64×10^4 s. Hence, for this case, the proposed method is over 5.3 times faster than the virtual voltage method. From these results, we can conclude that the proposed method could be effective especially for a large-sized shielding current analysis in an HTS film containing cracks.

4. Application to SPM

By using the method explained above, a high-speed numerical code has been developed for analyzing the time evolution of j . A typical j -distribution is shown in Fig. 3. In this section, we numerically investigate detectability of cracks by the SPM.

4.1 Model of SPM

An HTS film is assumed to have a rectangular cross section Ω of length l and width w , and cross sections of cracks are assumed to be line segments of length L_c . In the following, the longitudinal direction of Ω is taken as x -axis.

In the SPM, a cylindrical permanent magnet of radius R and height H is moved along the film surface and, simultaneously, an electromagnetic force F_z acting on the film is monitored. During the movement of the magnet, the distance L between the magnet bottom and the film surface is kept constant (see Fig. 1 in [4]). In the following, the symmetry axis of the magnet is denoted by $(x, y) = (x_A, y_A)$, and its movement is assumed as $x_A = \pm(vt - l/2) \equiv x_\pm(t)$ and $y_A = \text{const}$. Here, v is a scanning speed. In other

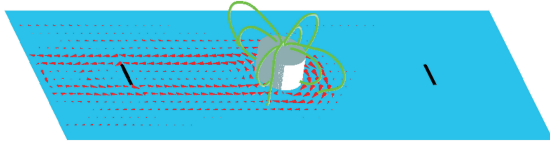


Fig. 3 The j -distribution for the same case as B ($a = 20$ mm) in Fig. 5. Here, the distribution is obtained at time satisfying $x_A = 0$ mm. In addition, the magnet movement is assumed as $x_A = x_+(t)$. In this figure, thick line segments and green curves denote cracks and magnetic flux lines, respectively.

words, the HTS film is scanned with the permanent magnet in two opposite directions.

Throughout the present study, the physical and geometrical parameters are fixed as follows: $R = 0.8$ mm, $H = 2$ mm, $L = 0.5$ mm, $B_F = 0.1$ T, $j_C = 1.0$ MA/cm², $E_C = 1$ mV/m, $N = 20$, $b = 1$ μ m, $l = 32$ mm, $w = 10$ mm, $L_c = 2$ mm, $y_A = 0$ mm, and $v = 10$ cm/s. Here, B_F/μ_0 is the magnitude of the magnetic field at $(x, y, z) = (x_A, y_A, b/2)$ for the case with $v = 0$ cm/s.

4.2 Crack detection using SPM

As a measure of crack detection, we use the defect parameter [4] defined by $d \equiv \text{sgn}(\Delta F_z^+ \cdot \Delta F_z^-) |\Delta F_z^+ \cdot \Delta F_z^-|^{1/2}$. Here, ΔF_z^\pm denotes a change in F_z due to cracks for $x_A = x_\pm(t)$ (double-sign corresponds). Since ΔF_z^\pm depends only on t and x_A is a monotonous function of t , ΔF_z^\pm becomes a function of x_A . Hence, the defect parameter d can be treated as a function of x_A .

Let us first investigate how the defect parameter is influenced by a single crack. The cross section of a crack is assumed to be a line segment connecting two points, $(0 \text{ mm}, \pm L_c/2)$, in the xy plane. The defect parameter d is calculated as a function of x_A and is depicted in Fig. 4. This figure indicates that the crack is contained in the shortest single interval $I(y_A)$ such that $I(y_A) \supseteq \{x_A : |d(x_A, y_A)| \geq \alpha, |x_A| \leq l/2\}$. Here, α is an infinitesimal positive constant. As is apparent from Fig. 4, a d - x_A curve is characterized by resolution $\rho \equiv |I(y_A)|$. If α is assumed as $\alpha = 2 \times 10^{-2}$ mN, we get $\rho \cong 5.9$ mm.

Next, we numerically investigate whether or not two cracks can be distinguished by the SPM. For this purpose, cross sections of two cracks are assumed to be the following two line segments in the xy plane: a line segment connecting two points, $(-a/2, \pm L_c/2)$, and a line segment connecting two points, $(a/2, \pm L_c/2)$. Here, a is the distance between two cracks. As explained above, resolution ρ of single-crack detection is about 5.9 mm. Hence, if the inequality $a \geq 5.9$ mm is satisfied, two cracks are expected to be separately detected by the SPM.

Dependences of the defect parameter d on x_A are numerically determined for $a = 10$ mm and for $a = 20$ mm, and they are depicted in Fig. 5. Contrary to expectations, the inequality $|d| < \alpha$ is not satisfied even at $x_A = 0$ mm

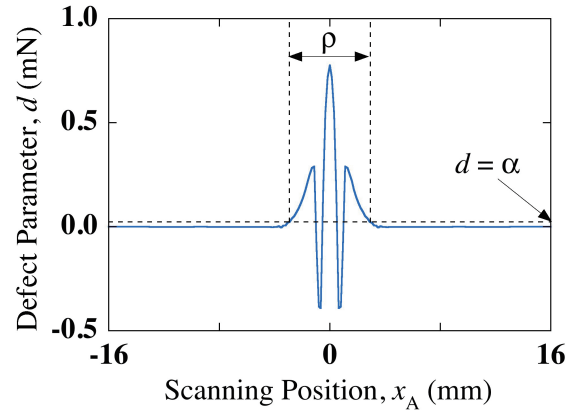


Fig. 4 Dependence of the defect parameter d on the scanning position x_A . Resolution ρ is also shown in this figure.

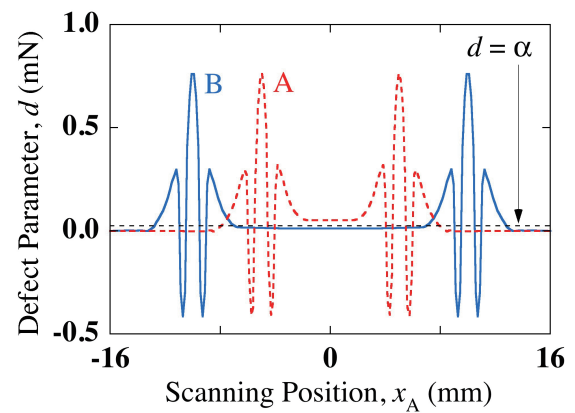


Fig. 5 Dependences of the defect parameter d on the scanning position x_A . Here, A: $a = 10$ mm and B: $a = 20$ mm.

for the case with $a = 10$ mm. In contrast, it is fulfilled there for the case with $a = 20$ mm. In other words, two cracks are regarded as a single crack for the case with $a = 10$ mm, whereas they are completely distinguishable for the case with $a = 20$ mm. This result implies that multiple cracks will remarkably affect resolution of the SPM.

5. Conclusion

We have investigated numerical methods for analyzing the shielding current density in an HTS film containing m cracks. After spatially discretized with n nodes, an initial-boundary-value problem of the shielding current density reduces to semi-explicit DAEs that can be written as ODEs. However, evaluation of function $f(t, \mathbf{T})$ on the right-hand side of the ODEs requires $O(n^3)$ operations because a linear system with a dense matrix needs to be solved at each evaluation. In order to accelerate function evaluations, we have proposed the method in which evaluation of $f(t, \mathbf{T})$ costs only $O((m+2)n^2)$ operations. A numerical code for calculating the shielding current density has been developed on the basis of the proposed method and, as an application of the code, detectability of cracks by the

SPM has been numerically investigated. Conclusions obtained in the present study are summarized as follows.

- The proposed method can be a powerful tool especially for a large-sized shielding current analysis in an HTS film containing cracks.
- If an HTS film contains multiple cracks, resolution of the SPM might be degraded remarkably.

Acknowledgment

This work was supported in part by Japan Society for the Promotion of Science under a Grant-in-Aid for Scientific Research (C) (No. 24560321, No. 26520204). A part of this work was also carried out with the support and under the auspices of the NIFS Collaboration Research program (NIFS13KNNTS025, NIFS13KNXN275).

- [1] Y. Yoshida, M. Uesaka and K. Miya, *IEEE Trans. Magn.* **30**, 3503 (1994).
- [2] A. Kamitani, T. Takayama and S. Ikuno, *IEEE Trans. Magn.* **47**, 1138 (2011).
- [3] A. Kamitani, T. Takayama and S. Ikuno, *IEEE Trans. Magn.* **49**, 1877 (2013).
- [4] A. Kamitani, T. Takayama, S. Ikuno and H. Nakamura, *Plasma Fusion Res.* **9**, 3405085 (2014).
- [5] W.H. Press, S.A. Teukolsky, W.T. Vetterling and B.P. Flannery, *Numerical Recipes in Fortran 77* (Cambridge Univ. Press, New York, 1992) p.708.
- [6] K. Hattori, A. Saito, Y. Takano, T. Suzuki, H. Yamada, T. Takayama, A. Kamitani and S. Ohshima, *Physica C* **471**, 1033 (2011).
- [7] R. Brambilla, F. Grilli and L. Martini, *IEEE Trans. Appl. Supercond.* **22**, 8401006 (2012).
- [8] A. Kameni, M. Boubekeur, L. Alloui, F. Bouillault, J. Lambrechts and C. Geuzaine, *IEEE Trans. Magn.* **50**, 7009204 (2014).